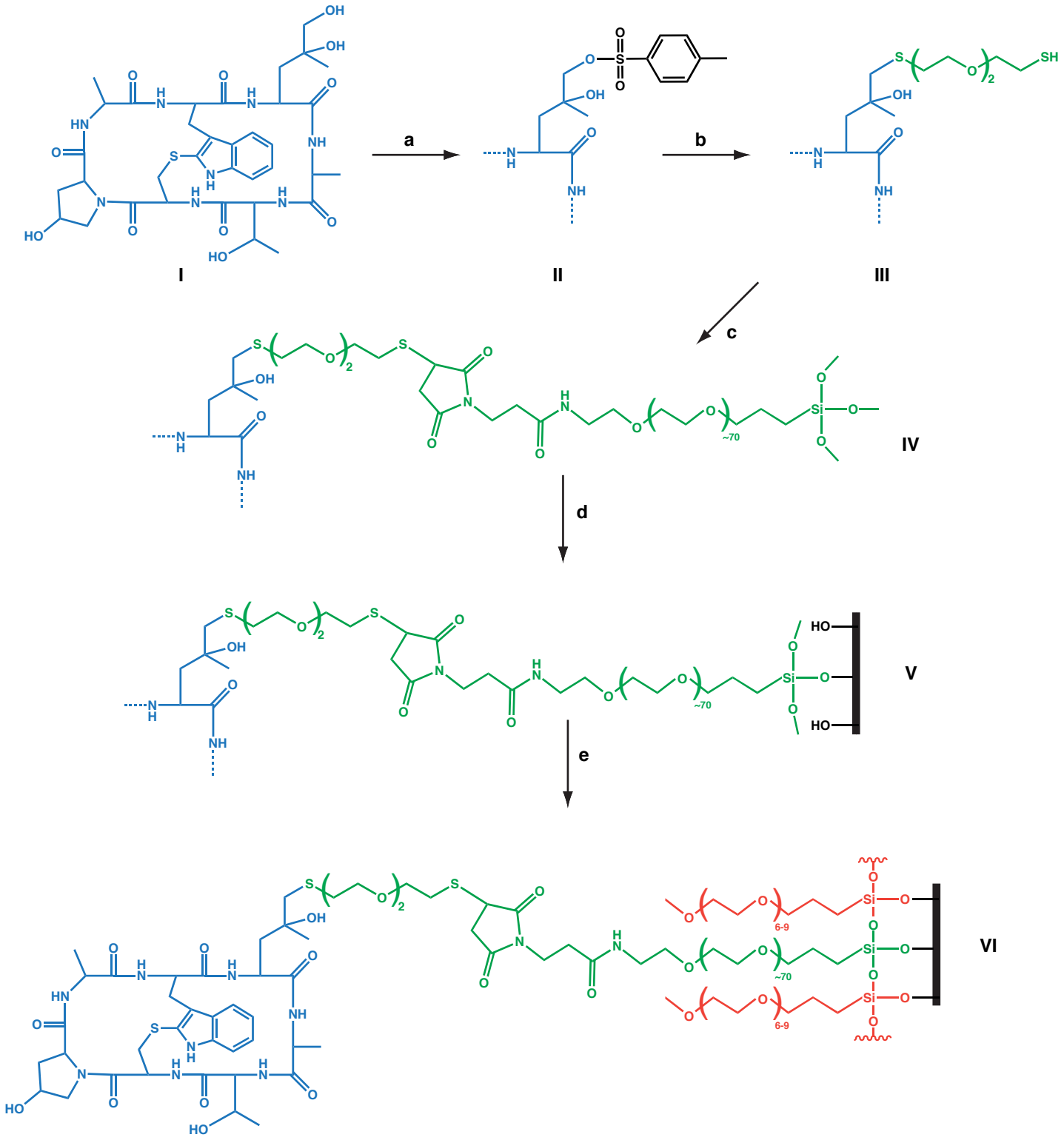

Figure S1 Synthesis of PEG-linked phalloidin and its coupling to superparamagnetic silica-coated particles.
See Methods for detailed conditions of the reaction steps. Phalloidin **(I)** was converted to mono-tosylated phalloidin **(II)** and reacted with a large molar excess of 1,8-dithiol-PEG_3 to form thiol-PEG_3-phalloidin **(III)**. This substance was converted to phalloidin-PEG-trimethoxysilane **(IV)** by addition of equimolar amounts of maleimido-$PEG_{\sim 70}$-trimethoxysilane. Any unreacted maleimide group was subsequently quenched by addition of a molar excess of $mPEG_6$-SH. Phalloidin-PEG-trimethoxysilane **(IV)** was immobilized to SiMAG silica beads to generate phalloidin beads **(V)**, which were surface passivated by the addition of an excess of 3-[Methoxy(PEG_{6-9})propyl]trimethoxysilane to give rise to the final surface passivated phalloidin beads **(VI)**. Control beads were treated identically except for the addition of thiol-PEG_3-phalloidin to the maleimide-PEG-silane.

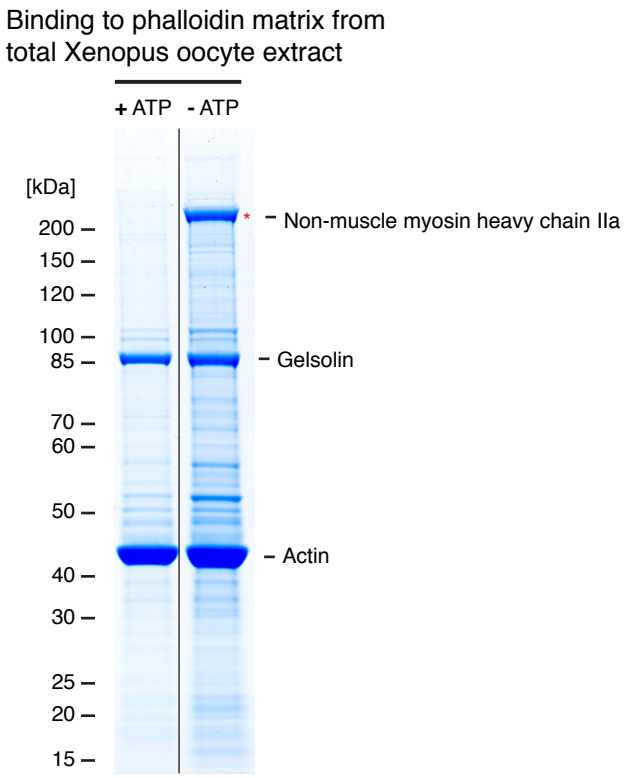

Figure S2 Analysis of F-actin complexes isolated from total Xenopus oocyte extract. Note that energy depletion by addition of apyrase prior to the wash step allowed co-purification of myosin motor proteins (Non-muscle myosin II band indicated by red asterisk). Gel has been cut as indicated by black line. In the standard reaction, a high phosphorylation potential was maintained by the addition of an energy-regenerating system containing 1 mM ATP and 20 mM creatine phosphate.

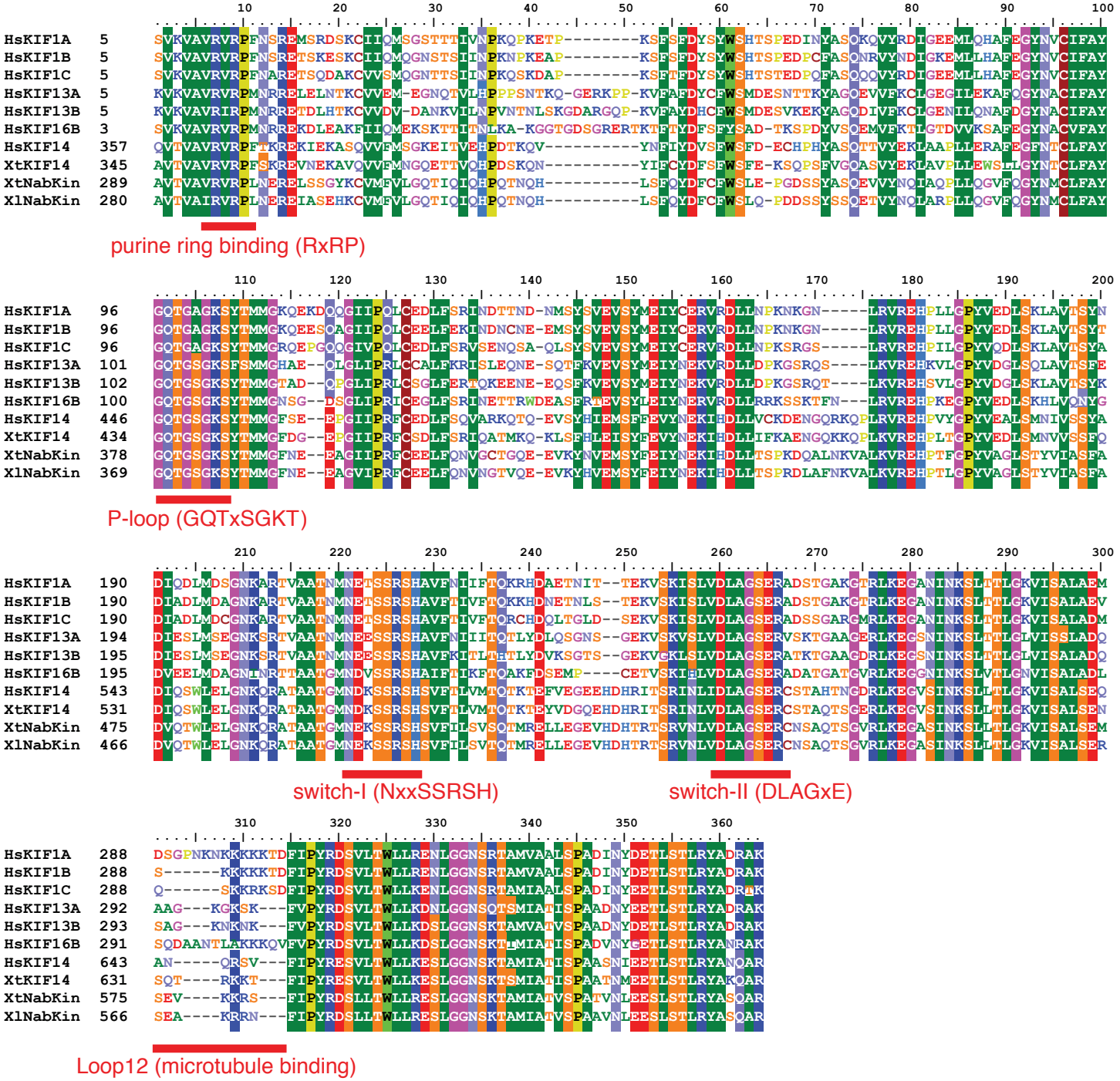

Figure S3 The motor domains of X.tropicalis KIF14 and NabKin and of X.laevis NabKin were aligned to human kinesin-3 homologs (KIF1, KIF13, KIF16, and KIF14). Motifs important for ATP-binding (purine ring binding and P-loop), ATP-hydrolysis (switch I and switch II) and microtubule binding (Loop12) are marked with red bars. The numbers on the left side denote the amino acid position within the full-length sequence. The human sequences have been derived from GenBank (KIF1A CAA62346, KIF1B AAI15396, KIF1C AAC52117, KIF13A AAG38890, KIF13B AAF81263, KIF14 BAA05392, KIF16A NM_020759, KIF16B AAO17292), the *Xl* NabKin has been sequenced in this study, and the *Xt* kinesins were derived by manual sequence assembly as described in the methods section.

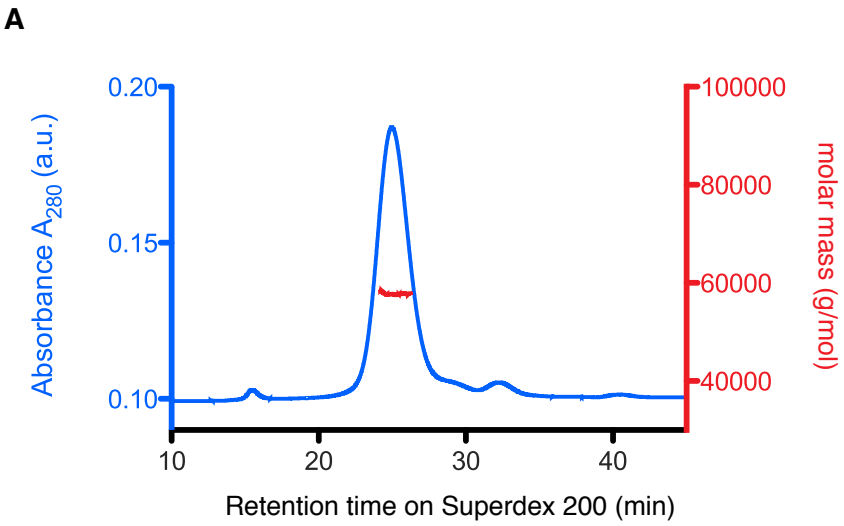

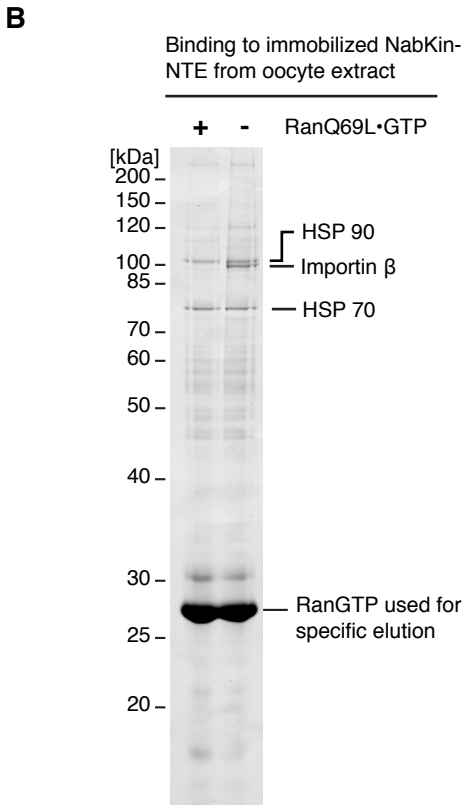

Figure S4

(A) Multi-angle light scattering analysis of an NabKin-NTE-EGFP fusion. This confirmed the monomeric state of the protein under F-actin binding assay conditions in the absence of F-actin (expected monomeric mass 56kDa). The measurement was performed on a Wyatt MiniDAWN TREOS machine coupled to a Sephadex 200 gel filtration column.

(B) Importin β binds NabKin-NTE in a Ran•GTP sensitive manner.

Complete lanes of Coomassie-stained SDS gel shown in Figure 3B. Proteins bound to the NabKin-NTE had been eluted with RanQ69L•GTP.

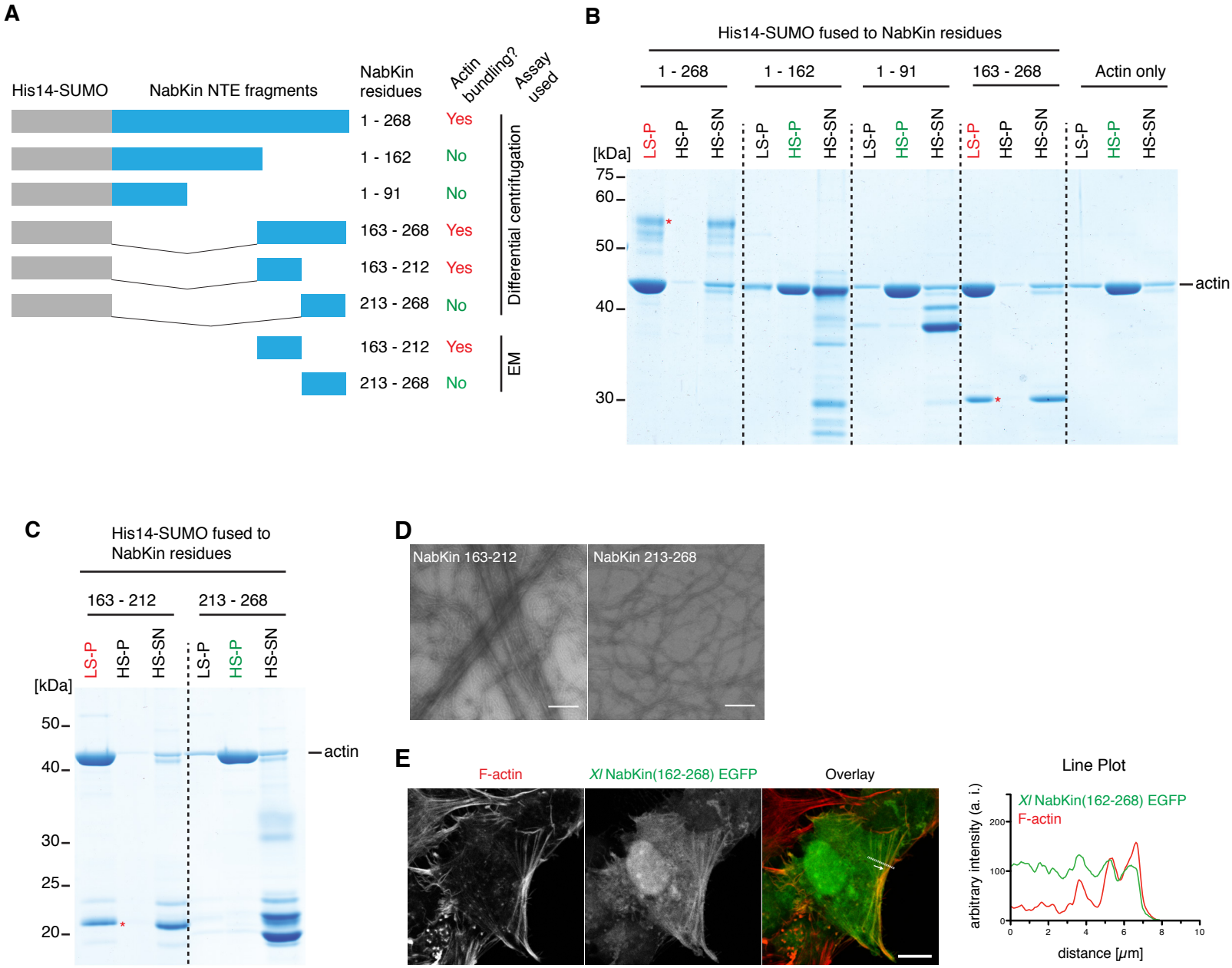

Figure S5 Mapping of the actin-bundling site within the NabKin NTE.
(A) Overview of the constructs analysed in (B) and (C).
(B) Differential centrifugation assay using truncations of the NabKin NTE and performed as outlined in Figure 2C.
(C) Differential centrifugation assay using truncations of fragment that was active for F-actin bundling in (B).
(D) Electron micrographs of negatively stained F-actin filaments that had been obtained in the presence of the indicated untagged segments of the NabKin-NTE. Scale bars = 200 nm.
(E) PtK2 cells expressing the minimal actin-bundling domain of NabKin (*X*/ NabKin 162-286) fused to the N-terminus of EGFP were fixed, stained for F-actin and DNA, and analysed by CLSM. Line plots represent pixel values along the dashed line. Scale bar = 10 μm.

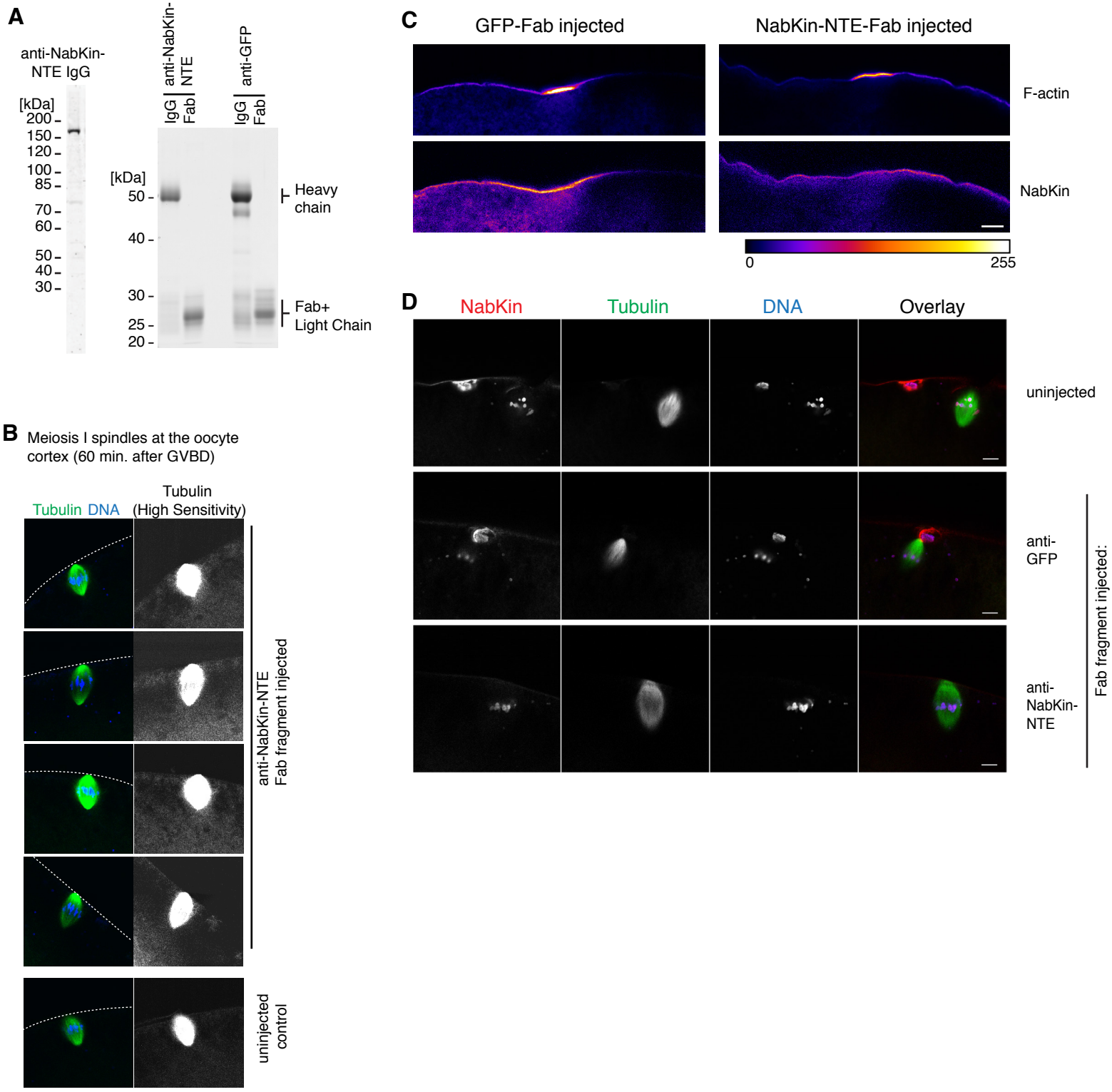

Figure S6 Fab-fragment injection inhibits NabKin localisation to actin-rich cortex.

(A) Immunoblotting using the anti-NabKin-NTE IgG on total oocyte extract (left). Unprocessed IgGs and Fab fragments of anti-NabKin-NTE and anti-GFP were analysed by SDS-PAGE and Coomassie staining (right).

(B) Meiosis I spindles at the oocyte cortex. Note that spindles in oocytes injected with anti-NabKin NTE Fab fragment were properly rotated and attached to the cortex as in control oocytes. High sensitivity recordings of tubulin were used to trace the oocyte cortex (represented by dashed line).

(C) NabKin displacement from the F-actin-rich cortex by NabKin-NTE-Fab-fragments. NabKin was detected by a cross-reacting antibody raised against the stalk of *Xt* KIF14 (*Xt* KIF14$^{783\text{-}1221}$) and an Fc-specific secondary antibody (Jackson ImmunoResearch, Inc.) to visualise NabKin independently of bound Fab-fragments. Scale bar = 10 μm.

(D) In Figure 7B, a secondary IgG (Alexa Fluor Goat Anti-Rabbit IgG (H+L); Invitrogen) recognising heavy and light chain (i.e complete IgGs and Fab fragments) was used for NabKin detection. To confirm the NabKin localisation by a Fab fragment-independent approach, we used the method detailed for panel C. The anti-rabbit Fc-specific secondary antibody seems to cross-react with the monoclonal mouse dsDNA antibody that we used for labelling chromosomes in this case. The DNA signal persisting after anti-NabKin-NTE Fab fragment injection therefore represents an internal control. Scale bar = 10 μm.

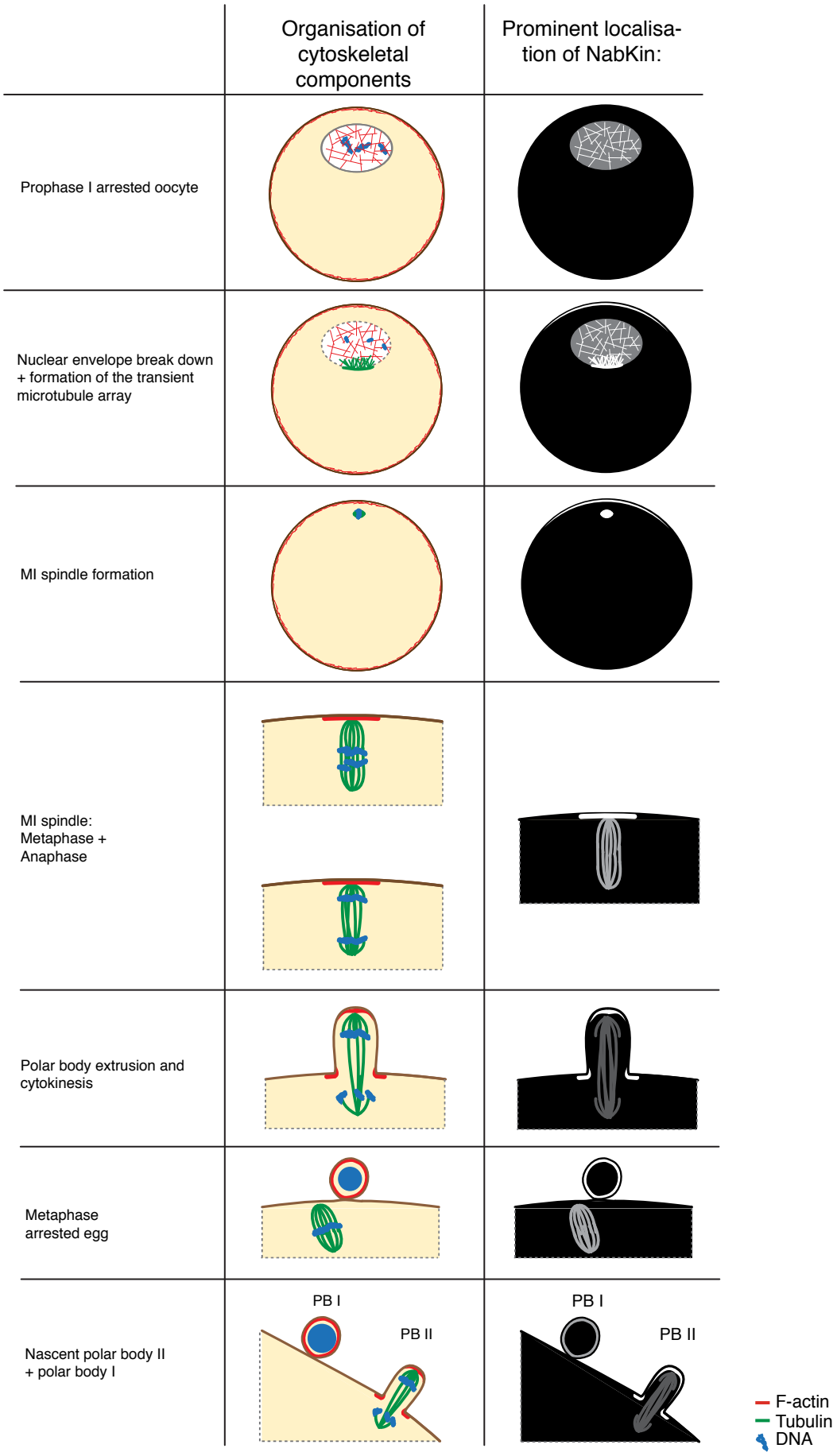

Figure S7 Summary of the cytoskeletal structures involved in Xenopus meiosis I and II and localisation of NabKin during these events. White staining indicates strong NabKin localisation, grey staining indicated weaker localisation.

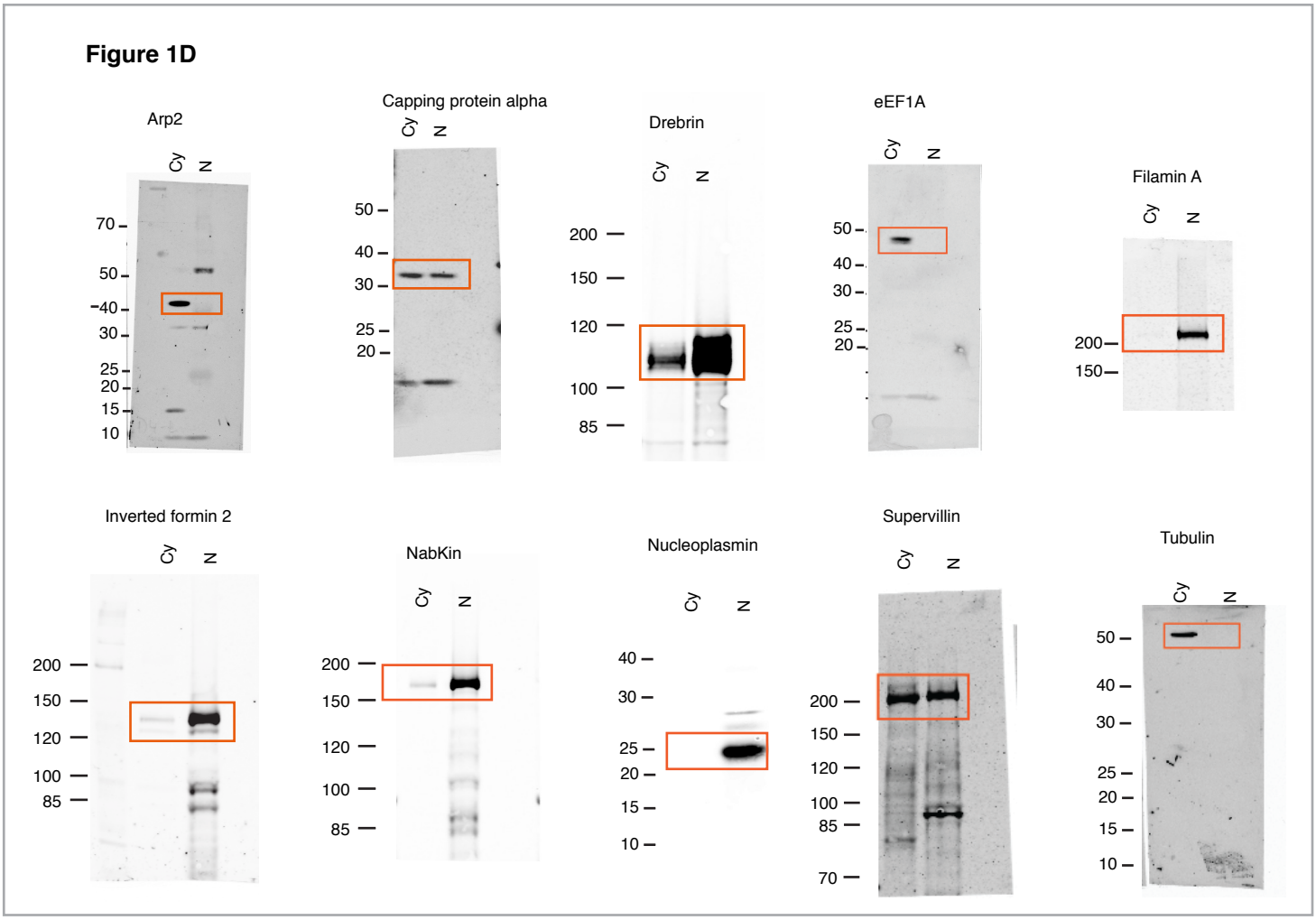

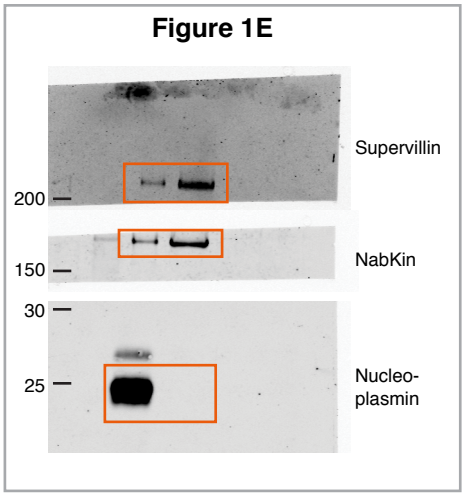

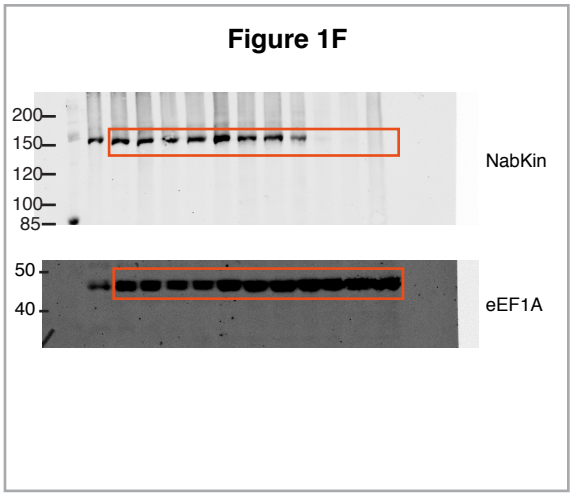

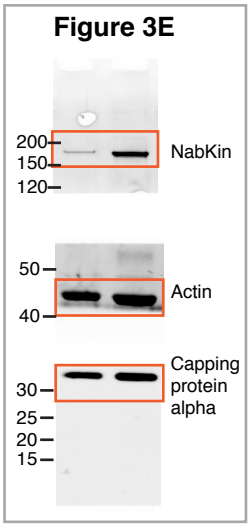

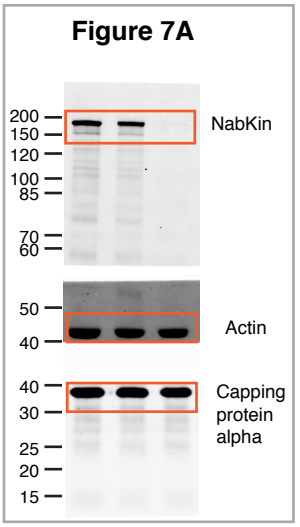

Figure S8 Full scans of the immunoblots presented in the paper. The rectangles indicate the images presented in the paper.

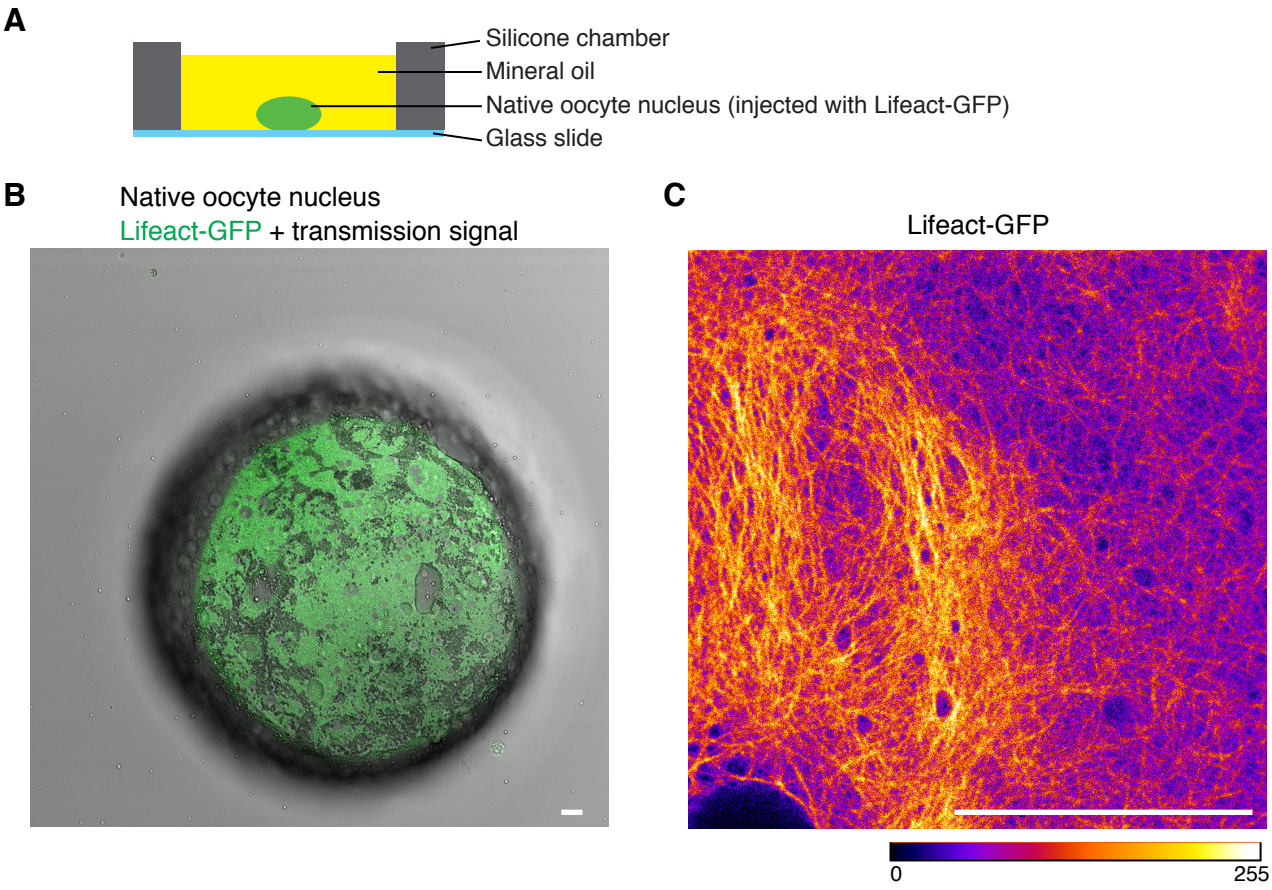

Figure S9 Visualisation of the F-actin network of a Xenopus oocyte nucleus isolated in mineral oil.
The oocyte was first transferred to Whatman paper to completely remove residual buffer and into mineral oil. The nucleus was then isolated, microinjected with 4.6 nl of a 6 μM Lifeact-GFP fusion (in 20 mM HEPES; pH 7.5), and imaged 30 min later while still being immersed in oil. Working in mineral oil avoids contact with exogenous buffers that might perturb the intranuclear F-actin network (Paine et al, 1992; Gall, 2006). LifeAct allows visualising F-actin with negligible alterations of actin dynamics (Riedl et al, 2008). Scale bar = 25μm.
(A) Scheme of the imaging setup.
(B) Image shows the isolated nucleus by a combination of the low magnification transmission signal with the LifeAct-GFP signal from a single confocal section.
(C) Image shows the LifeAct signal of the same nucleus in false-colour and at higher magnification.